$f(\alpha)$ curves: Experimental results

James A. Glazier, Gemunu Gunaratne, and Albert Libchaber
The James Franck Institute and Department of Physics, The University of Chicago, Chicago, Illinois 60637
(Received 10 July 1987)

We study the transition to chaos at the golden and silver means for forced Rayleigh-Bénard (RB) convection in mercury. We present $f(\alpha)$ curves below, at, and above the transition, and provide comparisons to the curves calculated for the one-dimensional circle map. We find good agreement at both the golden and silver means. This confirms our earlier observation that for low amplitude forcing, forced RB convection is well described by the one-dimensional circle map and indicates that the $f(\alpha)$ curve is a good measure of the approach to criticality. For selected subcritical experimental data sets we calculate the degree of subcriticality. We also present both experimental and calculated results for $f(\alpha)$ in the presence of a third frequency. Again we obtain agreement: The presence of random noise or a third frequency narrows the right-hand (negative q) side of the $f(\alpha)$ curve. Subcriticality results in symmetrically narrowed curves. We can also distinguish these cases by examining the power spectra and Poincaré sections of the time series.

I. INTRODUCTION

For certain combinations of temperature difference, aspect ratio, and external magnetic field, forced Rayleigh-Bénard (RB) convection in mercury exhibits dynamics similar to those of the critical circle map.[1] In this paper we carry out a detailed study of the transition to chaos in this system, and examine the effects of noise and of a third, nominally incommensurate, frequency. We use the $f(\alpha)$ singularity spectrum[2] and the power spectrum to compare the dynamics of the experiment with that of the circle map.[3]

Experimental studies of the transition to chaos in hydrodynamic systems have employed power spectra, Poincaré sections, Lyaponov exponents, and calculations of fractal dimension to characterize the states examined.[4] Previous work using the $f(\alpha)$ technique of characterizing attractors naturally tended to follow the same lines, concentrating on the $f(\alpha)$ curve exactly at criticality.[1,5–7] This focus made sense since exact theoretical results were known only for the critical cases.[1,2] The $f(\alpha)$ curves obtained from the RB system at criticality and with golden mean winding number agreed well with those obtained by exact calculations on the circle map,[1] confirming the correspondence between forced RB convection and the one-dimensional circle map already noted using other techniques.[8,9] Similar agreement obtained between the period-doubling cascades observed inside locked tongues in forced RB convection and the standard bifurcation tree.[5] One problem with these results was that the method of calculation employed was cumbersome (requiring a separate calculation for each q) and not terribly accurate. Thus only data sets already known to be critical from other tests were analyzed.

However, a better general understanding of the $f(\alpha)$ function has led us to develop improved techniques for calculating it from experimental data.[10] There are now good numerical $f(\alpha)$ curves for the subcritical circle map[11] and dynamical systems in the presence of noise are also better understood.[12] Thus we are able for the first time to carry out the experimental program proposed by Jensen *et al.*[1] In this paper we examine experimentally the regions around criticality, both subcritical and supercritical, and the effects of noise (in this case a third frequency) on the $f(\alpha)$ function. We also present a variety of spectra and Poincaré sections to show how these various techniques can reveal different aspects of the system's behavior.

II. EXPERIMENTAL PROCEDURE

The experimental apparatus consists of a rectangular cell, $0.7\times0.7\times1.4$ cm^3 filled with mercury. We maintain a constant vertical temperature difference across the cell to induce the oscillatory instability (this defines the internal frequency $f_{\rm int}$, typically 0.24 Hz), apply a constant magnetic field of approximately 240 G parallel to the short axis of the cell, and inject an alternating current (amplitude $A_{\rm ext}$, frequency $f_{\rm ext}$) asymmetrically through the mercury. The Lorentz force induced by the current couples nonlinearly to the vorticity field. We observe the state of the system by measuring the temperature as a function of time at the bottom center point of the cell. The experimental apparatus has been described in more detail elsewhere.[8]

In this experiment we attempt to set the winding number, $f_{\rm int}/f_{\rm ext}$, equal to either the golden [$\sigma_G=(\sqrt{5}-1)/2$] or silver ($\sigma_S=\sqrt{2}-1$) means. Because forced RB convection exhibits frequency locking, these ratios cannot be achieved exactly but can be approximated (to the accuracy allowed by experimental noise) by locking successively to the Fibonacci approximants (5/8, 8/13, 13/21, 21/34, . . . for σ_G and 5/12, 12/29, 29/70, 70/169,. . . for σ_S). A detailed description of the tuning process at the golden mean has been given elsewhere.[9]

Because of the rapid increase in denominator of the σ_S series, the silver mean is much more difficult to tune accurately than the golden mean. A particular problem in the silver-mean case, especially near and above criticality, is the noise or drift-induced transition between locked states which results in time variation of the winding number and hence limits the usable time series to a few hundred points. Because the silver mean is close to the strong resonance at $\frac{1}{2}$, silver-mean forcing drives higher-order instabilities more strongly than the golden mean and hence is more likely to produce unwanted additional frequencies.

The analyses presented here are based on stroboscopies, i.e., sequences of data $\{T_1,\ldots,T_n\}$, where $T_i \equiv T(t_0+i/f_{\text{ext}})$. We filter the raw data to eliminate long-term drift, using both a Krohn-Hite Model 3342 analog bandpass filter (cutoffs set at 0.01 and 10 Hz, 48 dB per octave) before sampling, and digitally after sampling. The digital filtering consists of subtracting off a flat running average from the digitized data. Because the data have intrinsic periodicity, the average is taken over 34 points for the golden-mean time series and over 29 points for the silver-mean time series, which are the approximate periods. We have checked that the filtering does not significantly affect the final $f(\alpha)$ curves obtained. The filtered data is then converted into the $f(\alpha)$ format using the method described in Sec. III and displayed as Poincaré sections (plots of T_i versus T_{i+1}). We also obtain power spectra of the unfiltered continuous time series using a Hewlett-Packard HP3562A spectrum analyzer.

III. CALCULATION OF THE $f(\alpha)$ SPECTRUM

Using the signal $\{T_i\}_{i=1}^{i=\infty}$ we first determine the rotation number of the circle map which corresponds to it by guessing a value for the rotation number Ω and graphing x_n versus $n\Omega \pmod 1$. For the correct Ω the graph is a one-dimensional curve.[10] Therefore using a series of trial Ω's, we do a binary search to determine the value that gives the most one-dimensional curve. This graph establishes the relationship (conjugacy) between the experimental curve and pure rotation and gives a natural ordering of points on the experimental curve. To nth order, the periodicity of the system is C_n, where C_n is the denominator of the nth continued-fraction approximant to the winding number; for example, for the golden mean C_n is the nth Fibonnacci number. Thus C_n gives the nth-order point of closest return and selecting a series of C_n points gives one approximate cycle.

Next, we use straight lines to approximate the curved arcs between successive points of the experimental data and obtain a partition of the curve. Since each of the arcs contains one point of the time series, each is equiprobable with probability $1/C_n$. Hence the probability measure and the arc lengths of each member of the partition are known. We use this partition to evaluate the generalized dimension and the singularity spectrum of the experimental curve. Note that the entire singularity spectrum is obtained from a single partition of the curve, involving one free parameter, the order of truncation of the continued fraction expansion.

More rigorously, the phase space of the experimental signal is three dimensional[1] (by the embedding theorem of Takens a circle map may be embedded in a space of dimension less than or equal to three), and hence the map

$$\mathbf{T}_{m+1}=\mathbf{F}(\mathbf{T}_m)\ , \tag{1}$$

where $\mathbf{T}_m=(T_m,T_{m+1},T_{m+2})$ is conjugate to a circle map, whose rotation number is denoted by Ω_0. Hence a graph of $\mathbf{G}=(m\Omega_0,\mathbf{T}_m)$, $(m=1,2,3,\ldots)$ is a one-dimensional curve, and so is any of its projections onto a plane.[10] In particular G, the graph of $(m\Omega_0,T_m)$ $(m=1,2,3,\ldots)$, is a one-dimensional curve. On the other hand, for an incorrect rotation number Ω this statement will generally not be valid and G will be space filling. If Ω is close to Ω_0 one can determine visually if it is smaller or larger than Ω_0 by looking at successive iterates. Therefore we determine Ω_0 by examining graphs of $(m\Omega_0,T_m)$ for several trial values of Ω, and iteratively refining Ω to obtain the most one-dimensional curve possible. Typically with a signal of about 1000 points we can determine Ω_0 to five significant figures and obtain results in perfect agreement with the frequencies given by the power spectra. Below criticality $\mathbf{G}$ is an invertible function while G is not. However, since G is a well-defined (i.e., single valued) function, the closest points on it correspond to closest points along $\mathbf{G}$. Further the order of points $(\mathbf{T}_{r(1)},\mathbf{T}_{r(2)},\ldots,T_{r(n)})$ on $\mathbf{G}$ is the same as that of $(T_{r(1)},T_{r(2)},\ldots,T_{r(n)})$ on G [we choose $r(1),r(2),\ldots,r(n)$ so that the corresponding points are consecutive along the curve]. We use this ordering to construct a partition on $\mathbf{G}$ that allows the evaluation of the generalized dimensions.

We determine the points of closest return by expanding Ω_0 in continued fractions. Denoting the nth continued-fraction approximant by p_n/q_n, the nth partition of the curve is the set of arcs S_m $(m=1,2,\ldots,q_n)$ between $\mathbf{T}_{r(m)}$ and $\mathbf{T}_{r(m+1)}$. For sufficiently large q_n the distance between $\mathbf{T}_{r(m)}$ and $\mathbf{T}_{r(m+1)}$ is small, and the arc can be approximated by a straight line. On the other hand, if S_m is too small, experimental noise will be important, and will lead to errors. For the system we study, choosing q_n between 100 and 500 gives optimal results. The optimum q_n can also be determined by evaluating the length of the curve, approximating the curve between $\mathbf{T}_{r(m)}$ and $\mathbf{T}_{r(m+1)}$ by a straight line. As q_n increases from 0 to about 100, the length increases as the length scale becomes sensitive to the curvature of $\mathbf{G}$. For q_n in the range 100–500 the length of the curve does not increase appreciably. For larger q_n the length again increases indicating that the length scale is comparable to the noise amplitude. The arcs S_m are equiprobable since they each contain one point of the set.

Hence, the probability measure of S_m is $p_m=1/q_n$ while its length is

$$l_m=(\mathbf{T}_{r(m)}-\mathbf{T}_{r(m+1)})\ . \tag{2}$$

The generalized dimension is $d_q=(q-1)\tau_q$ satisfies

$$1=\Gamma_n=\sum (p_m^q)/(l_m^{\tau_q})=q_n^{-q}\sum l_m^{-\tau_q} . \quad (3)$$

The singularity spectrum is the Legendre transform of τ_q, given by

$$\alpha=\frac{d\tau}{dq} ,$$

$$f(\alpha)=\alpha q-\tau(q) .$$

The convergence of τ_q for $q\rightarrow\infty$ is slow, so the convergence of the right-hand section (negative q) of the singularity spectrum is slow as well. The spectra for different values of q_n agree on all but the right (negative q) ends of the curves. In principle we can improve the convergence of τ_q by equating Γ_n and Γ_{n+1} and then solving, but the values so obtained are very sensitive to noise and cannot be used on experimental data.

The singularity spectrum for the trivial circle map (i.e., pure rotation) whose rotation number is the golden mean is a single point (1,1), and that for a critical circle map is the dashed curve shown repeatedly in Fig. 1 (column 1). The $f(\alpha)$ curve becomes wider near criticality, and the abscissa of the maximum moves to about 1.1. We find numerically that the addition of random noise makes the curve thinner, particularly for large values of α. The same conclusions hold if we add low amplitude noise consisting of a well-defined third frequency which is present in the indicated experimental runs [Fig. 1 (e1)–(e3)]. Above criticality the $f(\alpha)$ curve narrows because of the overlapping of the locked tongues and the appearance of large amplitude broadband noise (see Fig. 2). The narrowing of the $f(\alpha)$ curve is consistent with previous observations that for chaotic states the spectrum is essentially that of the quasiperiodic state with the addition of random noise.[1,9] In the frequency spectrum, the number of combination peaks decreases (i.e., the scaling of the spectrum becomes less critical) and the noise amplitude increases with the distance above criticality. We also note that the one-dimensional model fails for large forcing amplitudes.[5] We are currently beginning additional work on this problem.

The singularity spectrum found by the equiprobable partition generally converges faster than that obtained from partition of constant box sizes. In addition the number of discretionary parameters required to obtain the $f(\alpha)$ curves is much smaller than in earlier methods.[1,5] For example, for a given data set, all the generalized dimensions are determined using the same partition of the circle.

Using different values of q_n gives slightly different curves. We believe that these errors are due to the noise in the experiment and the slow convergence of the generalized dimensions for large negative q. The error bars in Fig. 1 (c1) and (c3) indicate this variation.

For subcritical states, the $f(\alpha)$ curve has a finite width only because of the finite number of points used for the calculation.[11] For a small number of points, the partition function is sensitive only to the larger distances along the attractor, which have nearly critical dynamics and yield an $f(\alpha)$ curve of finite width. Increasing the number of points systematically probes smaller length scales at which the structure is closer to pure rotation. Hence the $f(\alpha)$ curve becomes thinner as the number of points used in the calculation increases. For very large n we should obtain the single point $f(\alpha)$ curve of pure rotation, but the presence of noise in the experimental data prevents us from taking the limit. Nevertheless, the subcritical $f(\alpha)$ curve is meaningful. It is essentially independent of the detailed method used in the computation and thus is reproducible. Also, it allows us to determine the distance of the system from criticality. For rotation numbers near σ_G it is known that the effective coupling k measured using the F_n-cycle (where F_n is the nth Fibonacci number) is proportional to α^{2n}.[13] Hence, the generalized dimensions and the singularity spectrum are functions of $(1-k)\alpha^{2n}$ and the difference of the generalized dimensions $D_q^{(n)}(k)$ from those obtained at criticality $D_q^{(n)}(k=1)$ is given by

$$\Delta D_q(n,k)=D_q^{(n)}(k)-D_q^{(n)}(k=1)=h_q(\alpha^{2n}(1-k)) , \quad (4)$$

where α is the parameter rescaling for golden-mean rotations, and F_n points have been used for the calculation[11] The function $h_q(\alpha^{2n}(1-k))$ is approximately proportional to $\alpha^{2n}(1-k)$, the proportionality constant A_q being a function of q only. Thus the function $\Delta D_q(n,k)$ will be the same for all subcritical data sets apart from the rescaling factor. Knowing the rescaling factor gives the value of k. For the experimental data we obtain $\Delta D_q(n,k)$ curves which have the same shape as those obtained directly from the iterated map. The value of k obtained is the coupling strength at which a circle map will give the same singularity spectrum as the experimental data. Thus we can determine the degree of subcriticality from the experimental data. This correspondence is particularly valuable, because in general in experimental systems the control parameters do not map in any obvious way onto the natural parameters of the iterated map. We are currently undertaking additional work on this problem.

IV. RESULTS

We present experimentally determined results for the golden mean in Fig. 1, columns 1 and 2, and for the silver mean in columns 3 and 4. We determine the approximate criticality of the signal from the spectrum. As the control parameter increases towards its critical value, the number and amplitude of combination peaks in the spectrum increases [Figs. 1 (a2–c2) and (a4–c4)]. Above criticality, broadband noise appears [Fig. 1(d2) and (d4)]. We may deduce much of the same information from the Poincaré section (a plot of the strobed time series as T_i versus T_{i+1}). In this case the approach to criticality appears as the wrinkling of an originally smooth 1D loop [Fig. 3(a)], which breaks up into two-

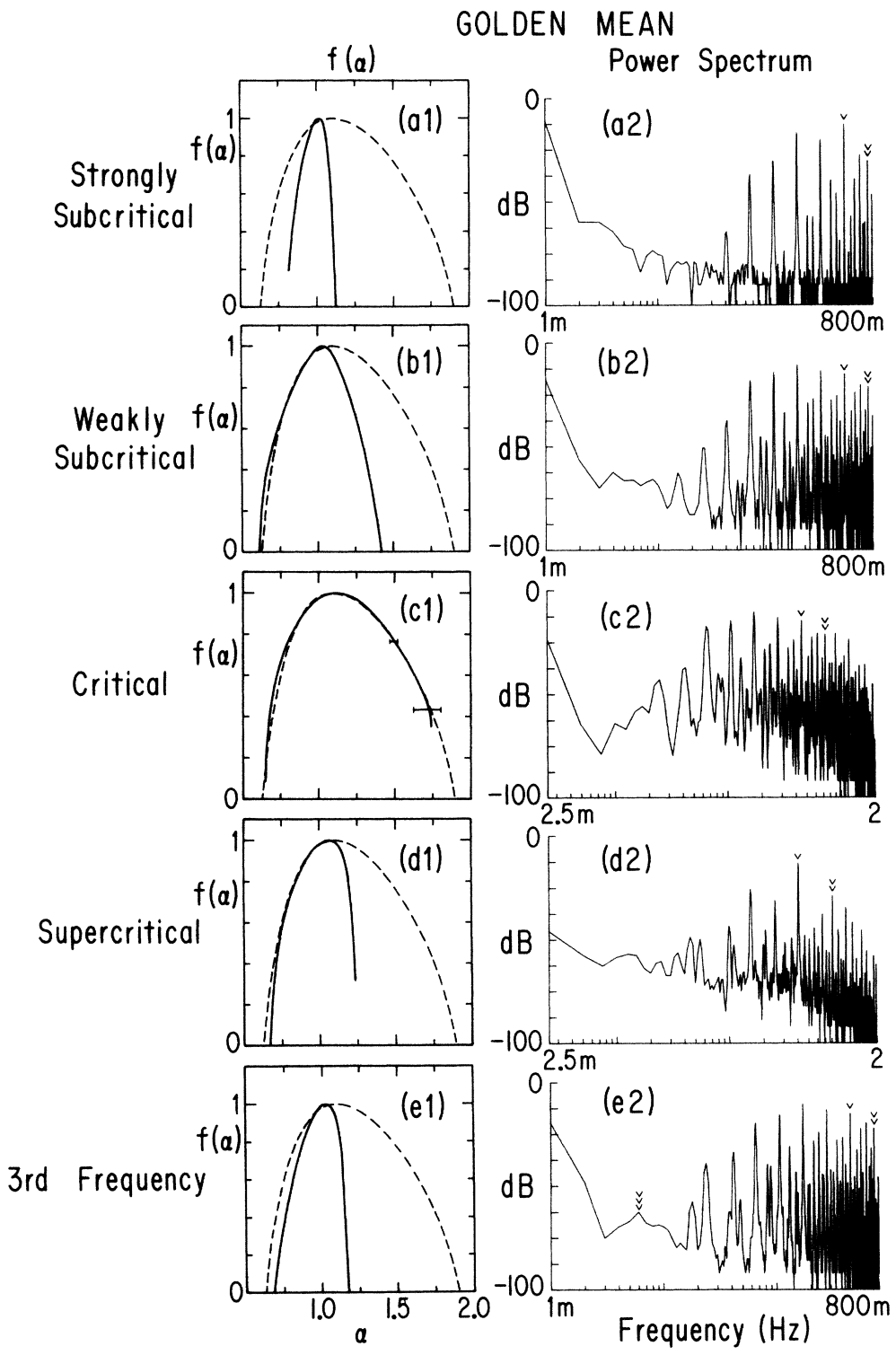

FIG. 1. Experimental spectra and $f(\alpha)$ curves at the golden and silver means: Column 1, golden-mean $f(\alpha)$ curves (dashed lines show numerically calculated critical curve); column 2, golden-mean spectra; column 3, silver-mean $f(\alpha)$ curves (dashed lines show numerically calculated critical curve); column 4, silver-mean spectra. Row a, strongly subcritical; row b, slightly subcritical; row c, critical; row d, supercritical; row e, third frequency present. In columns 2 and 4, single arrows mark the frequency of the oscillatory instability (f_{int}), double arrows the forcing frequency (f_{ext}). In (e2) and (e4), triple arrows mark the third frequency. The number of points used to calculate the $f(\alpha)$ curves were (a1), 89; (b1), 144; (c1), 377; (d1), 383; (e1), 123; (a3), 169; (b3), 233; (c3), 169; (d3), 79; (e3), 70. The equivalent couplings are (a1), 0.960; (b1), 0.977; (c1), 0.995. Note the ω^2 scaling in (c2). The error bars indicated in (c1) and (c3) are maximal deviations. For other figures the errors are typically a few percent.

dimensional fuzz above criticality [Fig. 3(b)]. For a fixed number of points, the computed length of the curve (as defined in Sec. III) increases abruptly at this transition.

In the experiment a third frequency may arise for a number of reasons: The convective flow may be naturally unstable to a low-frequency pattern competition oscillation, the external forcing may drive a pattern competition resonance which would not appear in the unforced state, or, as described in detail in an earlier paper, the third frequency may arise from a multifurcation of a su-

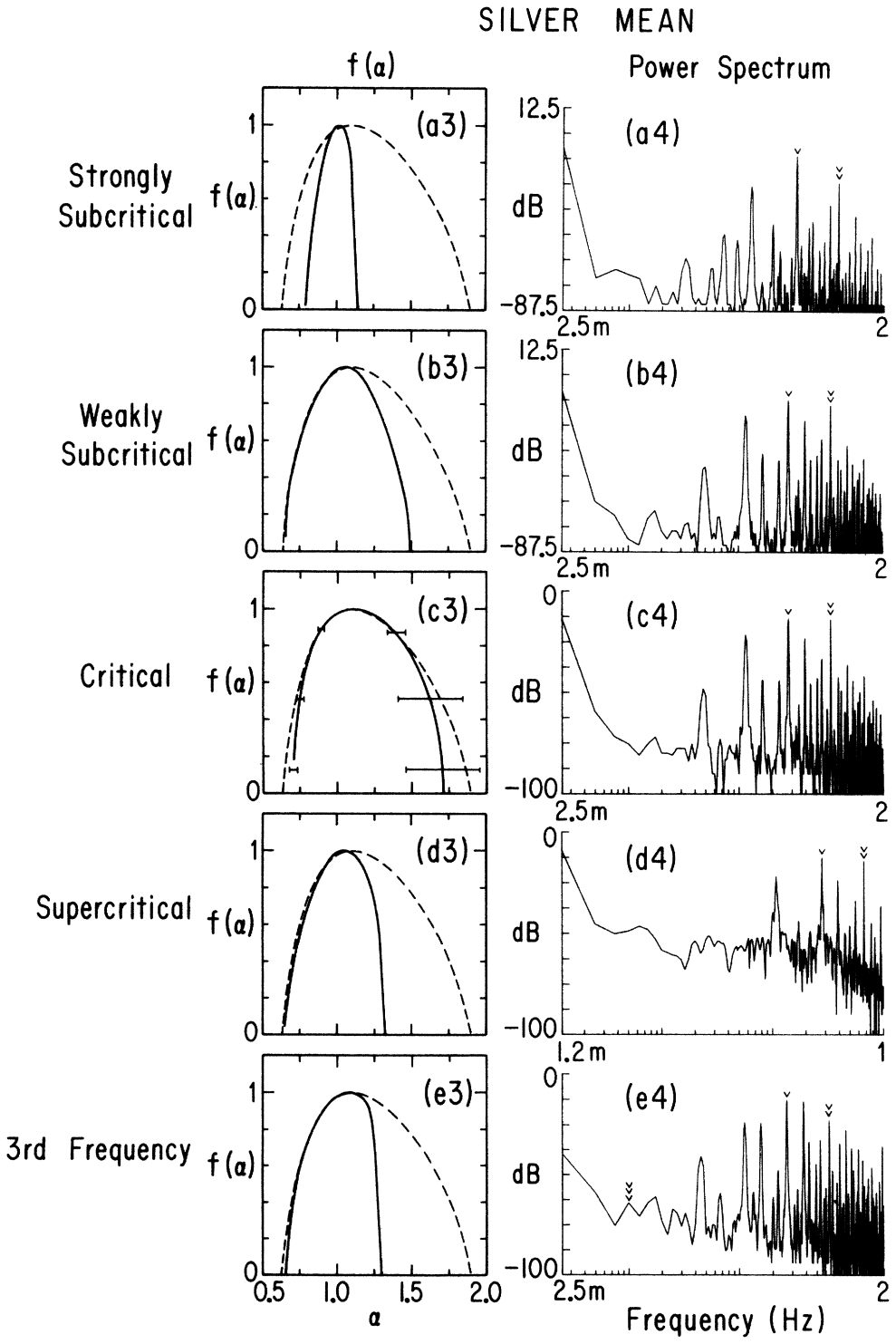

FIG. 1. (*Continued*).

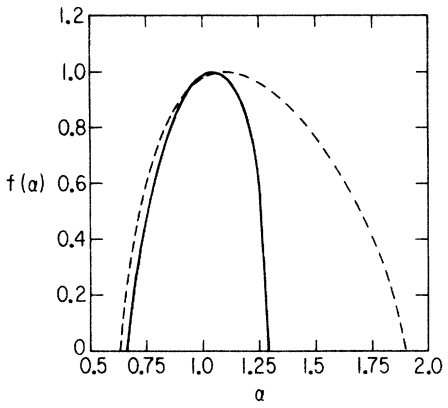

FIG. 2. Numerical $f(\alpha)$ curve: $f(\alpha)$ spectrum for a supercritical state near the golden mean using 144 points. The curve narrows asymmetrically, pulling in chiefly on the negative q side.

percritical locked state.[5] In all three cases, the low frequency dresses the main peaks as seen in Fig. 1 (e2) and (e4). Because the silver mean is close to the strong resonance at $\frac{1}{2}$, the resulting third frequency can be so strong that it dominates the spectrum completely (Fig. 4). The Poincaré sections help to distinguish the nature of the third frequency. The first two cases, when incommensurate or in a high locked state, produce a characteristic smeared Poincaré section [Fig. 3(c)]; when in a low-order locked state they produce a braided pattern of one-dimensional loops. Multifurcation of high-denominator locked states also produces a braided pattern [Fig. 3(d)].

With these qualitative features in mind we may turn to the calculation of the $f(\alpha)$ curves. On the basis of the previously demonstrated correspondence between the forced RB system and the circle map we expect that the $f(\alpha)$ curves will agree at criticality. A calculation at the golden mean has already been published.[1] We find excellent agreement at both the golden and silver means [Fig. 1 (c1) and (c3)]. The slight narrowing observed at the lower right of the curve, corresponding to large negative q values, is expected due to unavoidable experimental noise and limited time series lengths. Below criticality we observe the narrow $f(\alpha)$ curves predicted by numerical simulation [Fig. 1 (a1), (b1), (a3), (b3)]. If we fix the number of points used in the partition function, the width of the $f(\alpha)$ curve increases monotonically with the forcing amplitude, reaching its maximum at criticality. For consistently chosen winding number and q_n, we never observe a curve significantly wider than the critical curve. Incorrect values of these parameters result in

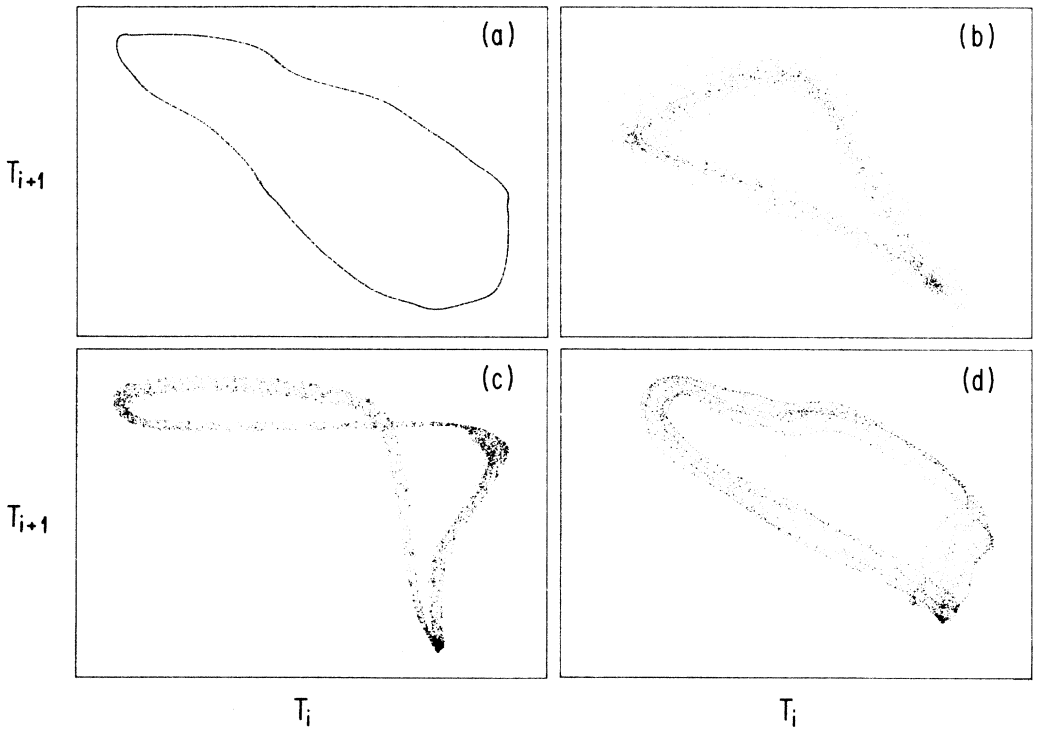

FIG. 3. Experimental Poincaré sections (plots of T_i vs T_{i+1} in arbitrary units): (a) subcritical; (b) supercritical; (c) third frequency present. Unlike the supercritical state, the smear is of uniform density, with well-defined edges. (d) Multifurcated. Note the presence of several one-dimensional curves.

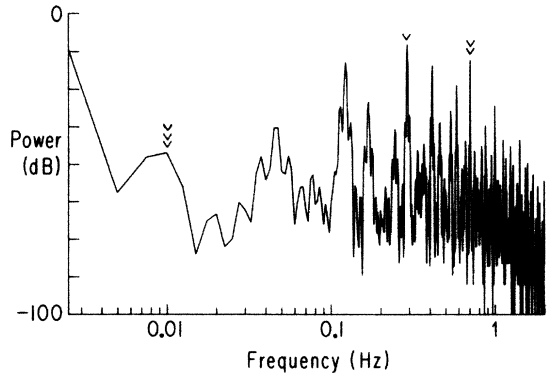

FIG. 4. Experimental spectrum: Subcritical silver-mean state with strong third frequency. Note that this is a locked state, so all frequencies are integer multiples of the lowest frequency. The single arrow marks the frequency of the oscillatory instability (f_{int}), the double arrow the forcing frequency (f_{ext}), and the triple arrow the third frequency.

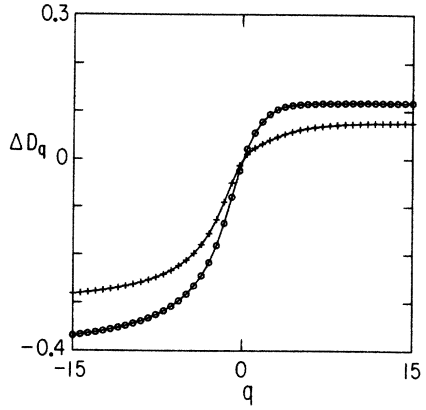

FIG. 5. Experimental $\Delta D_q(n,k)$: Curve is plotted as a function of q for two subcritical data sets. Apart from a rescaling these are identical to Fig. 4 of Ref. 11. This rescaling factor has been used to determine the equivalent coupling of the data. The curve indicated by circles is obtained using 377 points and its coupling is estimated to be 0.994, while that marked by crosses is obtained using 89 points and its coupling is 0.978.

wildly divergent $f(\alpha)$ curves. As predicted numerically (see Fig. 2), the supercritical case exhibits an $f(\alpha)$ curve narrowed on the negative q side [Fig. 1 (d1) and (d3)]. We also observe that the $f(\alpha)$ curve for subcritical data is insensitive to noise, but that it becomes more sensitive near criticality. Very near criticality the $f(\alpha)$ curves have sizable error bars, while away from criticality the errors are insignificant.

The location of the peak of the $f(\alpha)$ curve shifts on the horizontal axis from $\alpha=1$ to $\alpha\approx 1.1$ as we approach the transition. In the presence of a third frequency [Fig. 1 (e1) and (e3)] we again observe narrowing of the negative q side of the $f(\alpha)$ curve, in agreement with our numerical results. The asymmetric narrowing due to noise allows us to distinguish subcritical from noisy curves.

Finally we use the $f(\alpha)$ curve to estimate the subcriticality of the experimental data, i.e., we find the coupling of the equivalent circle map. In Fig. 5 we show $\Delta D_q(n,k)$ as a function of q for two subcritical data sets. We notice that these curves are proportional to those shown in Fig. 4 of Ref. 11. By comparing the scale of this curve with that of a numerically obtained curve of known coupling we estimate the value of k. For the curves of Fig. 5 the couplings (k) are 0.978 (crosses) and 0.994 (circles). For the data sets shown in Fig. 1 (a1), (b1), (c1) the equivalent couplings (k) are estimated to be 0.960, 0.977, and 0.995, respectively. We can in principle establish a relation between the scaling exponent of the spectrum and k, though we have not yet done so.

V. CONCLUSION

We have studied the transition of an experimental system from subcritical to supercritical motion. Though the experimental hydrodynamic system has many potential degrees of freedom, its phase-space behavior is low dimensional, its Poincaré map corresponding to a dissipative circle map embedded in three dimensions [see Fig. 3 (a)]. We have found that the local scaling properties are those of the circle map by comparing the power spectra and the singularity spectra, though the noise in the experiment narrows the $f(\alpha)$ spectrum slightly on the negative q side. The power spectra $A(\omega)$ for critical circle maps at the golden mean are proportional to ω^2, in agreement with experimental observation [Fig. 1 (c2)].[3] The experimental and theoretical singularity spectra agree well at criticality. The presence of noise or a third frequency makes the curves thinner (as seen numerically). When supercritical, the maps are noisy and tend to lock on to nearby periodic orbits, resulting in narrowed $f(\alpha)$ curves [Fig. 1 (d1) and (d3)], again agreeing with numerical results (Fig. 2).

We conclude that forced RB convection is (locally) conjugate to a circle map not only at criticality but for a large range of parameters and we can use the rescaling of $\Delta D_q(n,k)$ to map the experimental parameters onto those appropriate to the circle map. The strong convergence of the renormalization group fixed point for critical circle maps makes this possible.[13] However, for supercritical motion the higher dimensionality of the motion becomes important as can be seen in Fig. 3(b) (also see Glazier *et al.*[5]). Such systems may be better modeled by dissipative maps in higher dimension. We are currently beginning an experimental study of this higher-dimensional behavior using unstable periodic points.[14]

ACKNOWLEDGMENTS

This work was supported by National Science Foundation (NSF) Grant No. DMR-83-16204 and U.S. Office of Naval Research Grant No. N00014-84-K-0312.

[1]M. H. Jensen, L. P. Kadanoff, A. Libchaber, I. Procaccia, and J. Stavans, Phys. Rev. Lett. **55**, 2798 (1985).

[2]T. Halsey, M. H. Jensen, L. P. Kadanoff, I. Procaccia, and B. I. Shraiman, Phys. Rev. A **33**, 1141 (1986).

[3]S. J. Shenker, Physica (Utrecht) **5D**, 405 (1982).

[4]A random list of representative papers might include G. Ahlers and R. P. Behringer, Phys. Rev. Lett. **40**, 712 (1978); H. L. Swinney, Physica (Utrecht) **7D**, 3 (1983); J. P. Gollub and S. V. Benson, J. Fluid Mech. **100**, 449 (1980); A. Arneodo, P. Coullet, C. Tresser, A. Libchaber, J. Maurer, and D. d'Humiers, Physica (Utrecht) **6D**, 385 (1983); H. Haucke, Y. Maeno, and J. C. Wheatley, in *Dimensions and Entropies in Chaotic Systems* (Springer-Verlag, Berlin, 1986), p. 198; A. Brandstäter, J. Swift, H. L. Swinney, A. Wolf, J. D. Farmer, E. Jen, and P. J. Crutchfield, Phys. Rev. Lett. **51**, 1442 (1983). A host of similar papers on electronic systems might be cited, particularly those of C. Jeffries and collaborators and R. M. Westervelt and collaborators.

[5]J. A. Glazier, M. H. Jensen, A. Libchaber, and J. Stavans, Phys. Rev. A **34**, 1621 (1986).

[6]E. G. Gwinn and R. M. Westervelt, Phys. Rev. Lett. **59**, 157 (1987); Z. Su, R. W. Rollins, and E. R. Hunt, Phys. Rev. A **36**, 3515 (1987).

[7]M. J. Feigenbaum, M. Jensen, and I. Procaccia, Phys. Rev. Lett. **57**, 1503 (1986).

[8]J. Stavans, F. Heslot, and A. Libchaber, Phys. Rev. Lett. **55**, 596 (1985).

[9]J. Stavans, Phys. Rev. A **35**, 4314 (1987).

[10]J. Stavans, S. Thomae, and A. Libchaber, in *Dimensions and Entropies in Chaotic Systems* (Springer-Verlag, Berlin, 1986), p. 207.

[11]A. Arneodo and M. Holschneider, Phys. Rev. Lett. **58**, 2007 (1987).

[12]A few early theory papers on the problem are J. P. Crutchfield and B. A. Huberman, Phys. Lett. **77A**, 407 (1980); J. P. Crutchfield, M. Nauenberg, and J. Rudnick, Phys. Rev. Lett. **46**, 933 (1981); B. Shraiman, C. E. Wayne, and P. C. Martin, *ibid.* **46**, 935 (1981). An early experimental investigation is H. Haucke, R. E. Ecke, Y. Maeno, and J. C. Wheatley, Phys. Rev. Lett. **53**, 2090 (1984).

[13]M. J. Feigenbaum, L. P. Kadanoff, and S. J. Shenker, Physica **5D**, 370 (1982).

[14]D. Auerbach, P. Cvitanovic, J. P. Eckmann, G. H. Gunaratne, and I. Procaccia, Phys. Rev. Lett. **58**, 2387 (1987).

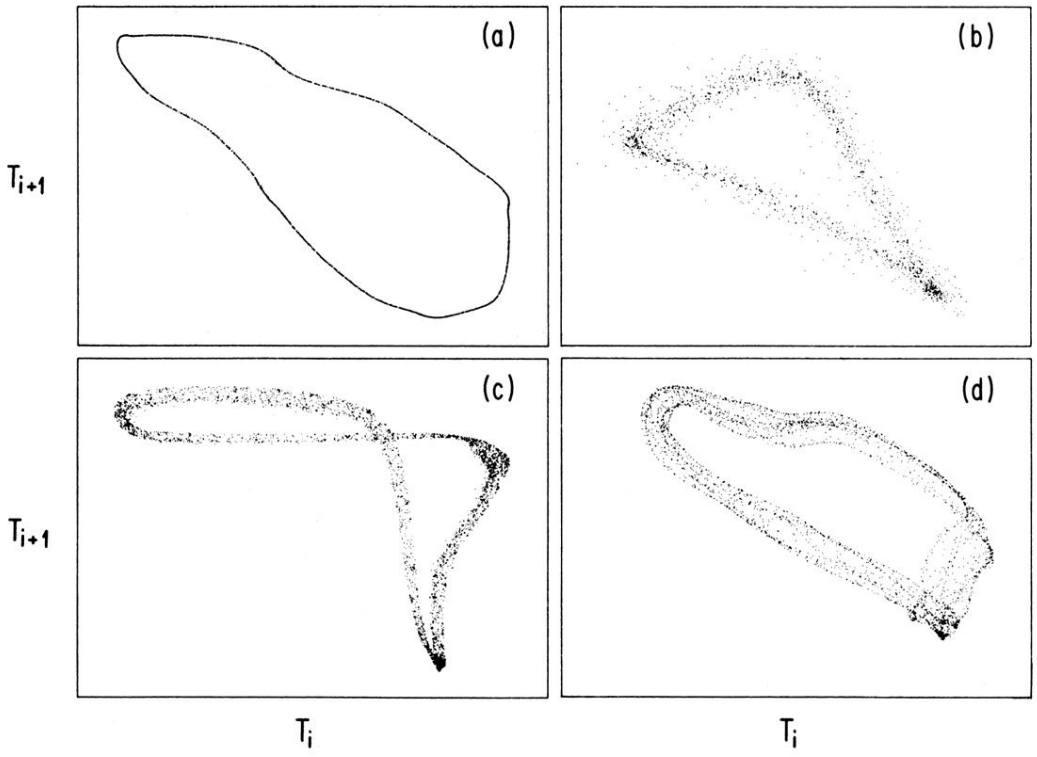

FIG. 3. Experimental Poincaré sections (plots of T_i vs T_{i+1} in arbitrary units): (a) subcritical; (b) supercritical; (c) third frequency present. Unlike the supercritical state, the smear is of uniform density, with well-defined edges. (d) Multifurcated. Note the presence of several one-dimensional curves.